Published in final edited form as:
Curr Biol. 2013 June 17; 23(12): 1037–1045. doi:10.1016/j.cub.2013.04.058.

GMF severs actin-Arp2/3 complex branch junctions by a cofilin-like mechanism

Casey A. Ydenberg[1,*], **Shae B. Padrick**[2,*], **Meredith O. Sweeney**[1], **Meghal Gandhi**[1], **Olga Sokolova**[3], and **Bruce L. Goode**[1,4]

[1]Rosenstiel Center for Basic Biomedical Research, Brandeis University, Waltham, MA, 02453

[2]Department of Biophysics, University of Texas Southwestern Medical Center, Dallas, TX 75390

[3]Faculty of Biology, Moscow State University, GSP-1, 1 Leninskie Gory, Bld 12, 119991, Moscow, Russia

Summary

Background—Branched actin filament networks driving cell motility, endocytosis, and intracellular transport are assembled in seconds by the Arp2/3 complex and must be equally rapidly debranched and turned over. One of the only factors known to promote debranching of actin networks is the yeast homologue of GMF, which is structurally related to the actin filament-severing protein cofilin. However, the molecular mechanism underlying debranching, and whether this activity extends to mammalian GMF, have remained open questions.

Results—Using scanning mutagenesis and TIRF microscopy, we show that GMF depends on two separate surfaces for debranching. One is analogous to the G-actin and F-actin binding site on cofilin, but we show using fluorescence anisotropy and chemical crosslinking that it instead interacts with actin-related proteins in Arp2/3 complex. The other is analogous to a second F-actin binding site on cofilin, which in GMF appears to contact the first actin subunit in the daughter filament. We further show that GMF binds to Arp2/3 complex with low nanomolar affinity and promotes the open conformation. Finally, we show that this debranching activity and mechanism are conserved for mammalian GMF.

Conclusions—GMF debranches filaments by a mechanism related to cofilin-mediated severing, but in which GMF has evolved to target molecular junctions between actin-related proteins in Arp2/3 complex and actin subunits in the daughter filament of the branch. This activity and mechanism are conserved in GMF homologues from evolutionarily distant species.

Keywords

Cytoskeleton; actin; ADF superfamily; Arp2/3 complex; GMF; yeast; mouse; disassembly; severing; debranching

[4]To whom correspondence should be addressed: MS029, Brandeis University, 415 South St, Waltham, MA, 02453. 781-736-2464, goode@brandeis.edu.
[*]These authors contributed equally to this work

Introduction

The rapid assembly and disassembly of branched actin filament networks nucleated by the Arp2/3 complex is responsible for driving the locomotion of a wide variety of cellular structures [1]. The Arp2/3 complex is a seven-subunit assembly consisting of two actin-like proteins and five unrelated proteins [2, 3]. When bound to a nucleation-promoting factor (NPF) of the WASp superfamily, it is capable of nucleating a new actin filament [4–6] from the side of a pre-existing mother filament [2]. Tomographic reconstructions of these branches show that Arp2/3 complex is stably associated with junctions, positioned such that the two actin-like subunits, Arp2 and Arp3, anchor the pointed end of the daughter filament [7]. This mechanism of Arp2/3 complex nucleation has been known for some time; however, much less is known about branched network pruning and disassembly.

For continuous growth and force-generation, branched actin networks must be turned over as rapidly as they are polymerized. The actin filament-severing protein cofilin/ADF (actin depolymerizing factor) plays one critical role in this process [8–10]. Cofilin binds cooperatively to actin filament sides and changes their twist by ~5° [11–14]. Severing occurs at the boundaries between cofilin-bound and –unbound regions [15]. Cofilin also has been proposed to remove Arp2/3 complex branch junctions [16, 17]. However, evidence suggests that this effect occurs via cofilin targeting the mother filament and not Arp2/3 complex itself [17].

Cofilin is part of a larger superfamily of proteins called actin depolymerizing factor homology (ADFH) proteins, which also includes twinfilin, Abp1/drebrin, coactosin, and GMF [18]. While these other ADFH proteins have all been implicated in regulating actin cytoskeleton dynamics, their biochemical activities and genetic phenotypes are not as well understood as those of cofilin. GMF family proteins do not interact with actin, but instead bind to Arp2/3 complex [19–21]. In reconstitution experiments, GMF isoforms from yeast and mammals inhibit actin nucleation stimulated by Arp2/3 complex and the VCA domain of WASp-family proteins [19, 21]. Remarkably, at much lower concentrations, yeast Gmf1/Aim7 [22] removes daughter filaments from their mothers without inducing severing events at other locations [19]. Thus, Gmf1 may sever at branch junctions. These observations have left open many important questions: Is GMF's debranching mechanism related to cofilin's filament severing mechanism? Is debranching a conserved function? How does GMF interact with Arp2/3 complex?

To address these questions, we performed scanning mutagenesis of yeast Gmf1 to define surfaces important for its in vivo and biochemical functions. This analysis revealed that Arp2/3 complex binding and nucleation inhibition by GMF depends specifically on a surface that is analogous to the surface of cofilin that binds both actin monomer and filament, which we term 'site 1'. Debranching requires an additional GMF surface that is analogous to a surface on cofilin that binds specifically to F-actin, which we term 'site 2' [23]. We extended these analyses to mouse GMFγ, and determined that debranching is a conserved function, and that a site 2 mutation similarly disrupts debranching without affecting inhibition of nucleation activity. A combination of biophysical, modeling and biochemical methods suggest that GMF prunes daughter filaments by a cofilin-related severing mechanism, in which GMF uses site 1 to bind to actin-related proteins in Arp2/3 complex, and site 2 to bind the first actin subunit in the daughter filament.

Results

Site-directed mutagenesis of Gmf1

To dissect GMF function, we generated six *gmf1* alleles based on homology to *cof1* alleles that have strong defects in cell growth and actin binding. Subsequently, we generated an additional 11 alleles that target clusters of charged or strongly conserved residues in GMF. Thus in total, we mutated 38 residues on Gmf1 within 17 different alleles (Fig 1A and Supplemental Table S1).

In yeast, deletion of *GMF1* exacerbates the growth defects of a *cof1-22* mutant, lowering the restrictive temperature from 37° to 34° C. Expressing Gmf1 under the *GMF1* promoter (from a low copy plasmid) in the *cof1-22 gmf1* Δ strain accelerates growth at 34° C (Fig. 1). By expressing our Gmf1 mutants instead of wild type, we identified six mutants that grew significantly slower than a strain carrying wild-type *GMF1* (Fig 1B and Supplemental Table S1). The mutated residues cluster in three distinct regions of the protein (Fig 1C). The first region, targeted by *gmf1-17* ($p = 0.03$) and *gmf1-20* ($p < 0.01$), corresponds to the same surface as site 1 of Cof1 [8] (Fig 1D and Supplemental Fig S1). The second region, targeted by *gmf1-101* ($p < 0.01$) and *gmf1-16* ($p < 0.01$), corresponds to the same surface as site 2 (Fig 1D and Supplemental Fig S1). The third region, targeted by *gmf1-103*, resides on a surface-exposed beta-strand adjacent to *gmf1-101*, and is not part of either site.

Debranching activities of mutant Gmf1 proteins

To better understand the activities that underlie *GMF1* cellular functions, we purified the mutant Gmf1 proteins that showed defects in vivo. The mutant Gmf1-103 could not be purified, thus the growth defect may arise from a folding problem. The folding stabilities of other Gmf1 mutant proteins were similar to wild type Gmf1 except for Gmf1-17 and Gmf1-16. These had about 8°C lower and 5°C lower denaturation midpoint temperatures (T_m), respectively (Supplemental Fig S2). Note that these T_m values are ~20°C higher than the growth temperature, and thus the proteins are most likely stable in vivo.

We compared the debranching activity of these Gmf1 proteins using real-time TIRF microscopy analysis of actin filament dynamics nucleated by yeast Arp2/3 complex and WASp VCA [19]. In reactions lacking Gmf1, branched filaments were rapidly nucleated, and debranching events were rare (Fig 2A; $1.0 \pm 0.5 \times 10^{-4}$ s^{-1}). We then performed this analysis in the presence of 20 nM Gmf1 or a mutant variant (Fig 2B). At this concentration debranching is readily detectable and sub-saturating [19], making the assay sensitive to differences in K_I. As previously shown [19], addition of wild-type Gmf1 accelerated the debranching rate by over 50-fold (Fig 2B–C; $5.5 \times 10^{-3} \pm 0.5 \times 10^{-3}$ s^{-1}).

Both site 1 mutants of Gmf1 were found to be defective in debranching to similar extents (Gmf1-17: $1.6 \times 10^{-3} \pm 0.2 \times 10^{-3}$ s^{-1}; Gmf1-20: $2.1 \times 10^{-3} \pm 0.4 \times 10^{-3}$ s^{-1}; Fig 2C and Supplemental Table S2). Gmf1-101 was more strongly defective in debranching ($7 \times 10^{-4} \pm 2 \times 10^{-4}$ s^{-1}). Gmf1-16 (site 2) was not significantly defective in debranching ($3.9 \times 10^{-3} \pm 0.8 \times 10^{-3}$ s^{-1}).

In addition to the mutants above, we purified Gmf1-4, which is a serine-to-glutamate substitution, as it targets a site reported to be phosphorylated in mammalian GMF [20]. We also purified Gmf1-105, because it targets a patch of acidic residues proximal to Gmf1-103. Gmf1-4 debranched as efficiently as wild-type Gmf1 (Fig 2C and Supplemental Table S2; $5.0 \times 10^{-3} \pm 0.8 \times 10^{-3}$ s^{-1}), while Gmf1-105 debranched at a modestly reduced rate ($2.6 \times 10^{-3} \pm 0.5 \times 10^{-3}$ s^{-1}), demonstrating that it is less impaired than any of the site 1 mutants. These results show a correlation between mutant deficiencies in complementing *gmf1* Δ in vivo and in debranching in vitro.

Inhibition of nucleation by Arp2/3 complex depends on site 1 of Gmf1

At higher concentrations, Gmf1 also binds to Arp2/3 complex in solution and inhibits Arp2/3 complex-mediated nucleation [19–21]. Therefore, we tested the mutant Gmf1 proteins for inhibition of nucleation by Arp2/3 complex. Wild-type Gmf1 robustly inhibited Arp2/3 complex-mediated nucleation (Fig 3A–B), whereas mutant Gmf1 proteins exhibited variable defects (Fig 3B and Supplemental Table S2). Gmf1-20 and Gmf1-17, both of which target site 1, were defective in Arp2/3 complex inhibition (note that Gmf1-17 and Gmf1-20 saturate at different degrees of inhibition; see Discussion). In contrast, Gmf1-16 and Gmf1-101, both of which target site 2, were not significantly impaired in Arp2/3 complex inhibition.

The results show that residues in site 1 are important for inhibition of nucleation by Arp2/3 complex. In contrast, site 2 does not appear to be important for inhibition of nucleation by Arp2/3 complex (Fig 3B), but it is critical for debranching (Fig 2C). Thus, Gmf1-101 uncouples debranching from Arp2/3 complex nucleation inhibition, and suggests that debranching requires additional molecular interactions (see Discussion). Curiously, our two pseudo-wildtype mutants (Gmf1-4 and Gmf1-105) were strongly defective in nucleation inhibition (Supplemental Table S2). This suggests that nucleation inhibition is not strongly correlated with in vivo defects and therefore that debranching may be the more important activity in yeast cells. Interestingly, Gmf1-16 showed no defects in nucleation inhibition or debranching despite causing strong defects in vivo (Fig 1), suggesting that this surface on Gmf1 may contribute to regulation and/or localization in vivo. Indeed, the analogous Cof1-16 site is implicated in PIP2 binding [24].

The mechanism of nucleation by Arp2/3 complex involves a number of steps, including a conformational change that brings the two Arp subunits into close proximity (known as the ‘closed’ conformation) [25]. We used negative stain electron microscopy to directly image Gmf1-GFP bound Arp2/3 complex. Individual Arp2/3 complex particles were picked and classified (Fig 3C). The class sums were used to determine the fraction of Arp2/3 complexes in three conformations (Fig 3D). Without Gmf1, 57.0% of Arp2/3 complex particles were open, 13.7% intermediate and 29.2% closed. Upon addition of Gmf1-GFP, 70.2% of the particles were open, 18.8% intermediate and 11.0% closed. (Fig 3D). This is consistent with Gmf1 shifting the conformational distribution of Arp2/3 complex away from the closed and towards the open structure (chi-squared test: $p < 0.01$).

Mouse GMFγinhibits nucleation by Arp2/3 complex and promotes debranching

Debranching activity has thus far been demonstrated only for yeast Gmf1. We therefore performed debranching assays using bovine Arp2/3 complex and purified *Mus musculus* GMFγ [20, 21]. This analysis revealed that GMFγ indeed stimulates debranching (Fig 4A), although it was less active than yeast Gmf1. We then introduced an alanine substitution in GMFγ at three residues (R19A K20A K22A), corresponding to the yeast Gmf1-101 (Fig 1A) allele that was defective specifically in debranching. As observed for yeast Gmf1-101, mouse GMFγ-101 strongly abrogated debranching activity (Fig 4A), demonstrating a mechanistic parallel between yeast and mouse GMFs.

We further compared the abilities of wild-type GMFγ and mutant GMFγ-101 to inhibit Arp2/3 complex-mediated nucleation. GMFγ and GMFγ-101 inhibited actin assembly by bovine Arp2/3 complex equally well (Fig 4B). Therefore, mouse GMFγ-101 exhibits similar properties to its yeast counterpart: it is strongly impaired in debranching but shows normal nucleation inhibition activity. Remarkably, mouse GMFγ could inhibit yeast Arp2/3 complex (Fig 4C), providing further evidence that the nature of the interactions between Arp2/3 complex and GMF is conserved across phylogenetic kingdoms.

Binding of Gmf1 to Arp2/3 complex

Our finding that Gmf1 site 1 is critical for the debranching and nucleation inhibition functions points to a possible interaction between Gmf1 and one or both actin-related protein subunits in Arp2/3 complex (Arp2 and/or Arp3). Indeed, in cofilin, site 1 binds to actin subdomains I and III [26], a region highly conserved among actin, Arp2, and Arp3 [27].

To determine the stoichiometry of Gmf1-Arp2/3 complex interactions, we performed multisignal sedimentation velocity analytical ultracentrifugation [28], following the sedimentation using Raleigh interference signals and absorbance at 492 nm. Gmf1 was tagged with GFP (referred to as Gmf1-GFP) [19], providing a unique signal at 492 nm. From sedimentation velocity data for these two signals (Fig. S3), $c(s)$ distributions were constructed for yeast Arp2/3 complex and Gmf1-GFP separately (Fig 5A). Free yeast Arp2/3 complex showed a sedimentation coefficient of 9.4 S (Supplemental Table S3), similar to the 9.2 S sedimentation coefficient reported for bovine Arp2/3 complex [29]. Free Gmf1-GFP sediments substantially more slowly than Arp2/3 complex (Fig 5A), consistent with it being present as a monomeric species. Similar experiments were performed for mixtures of Gmf1-GFP and Arp2/3 complex (Supplemental Fig S3D and E), and $c_k(s)$ distribution were fit for Arp2/3 complex and Gmf1-GFP (Fig 5B). These distributions show that the Arp2/3 complex sediments more rapidly in the presence of Gmf1-GFP (Fig 5B and Supplemental Table S3) and a portion of Gmf1-GFP cosediments with Arp2/3 complex.

By optimizing the ratio of Gmf1-GFP that cosediments with Arp2/3 complex in fitting (Supplemental Fig S3F and G), we estimated the stoichiometry of Gmf1-GFP association with Arp2/3 complex. This was performed for a range of Gmf1-GFP concentrations in the presence of approximately 700 nM Arp2/3 complex. The observed stoichiometries (Supplemental Table S3 and Supplemental Fig S3J) indicate two binding sites for Gmf1 on Arp2/3 complex. In particular, a stoichiometry of ~2 Gmf1-GFPs per Arp2/3 complex is seen when ~3.5 μM unbound Gmf1-GFP is present. Sub-stoichiometric concentrations of Gmf1-GFP bound Arp2/3 complex completely, consistent with the first binding site having a K_D tighter than 30 nM (Supplemental Fig S3H). At high Gmf1-GFP concentrations, additional bound and free Gmf1-GFP is observed (Fig 5B), consistent with a second, lower affinity binding site. Assuming two asymmetric binding sites for GMF on Arp2/3 complex, and using isotherms from effective particle theory [30], the K_D of the second Gmf1-GFP binding site is estimated to be ~2 μM (Supplemental Fig S3I and J and Supplemental Table S3).

Next, we measured the Arp2/3 complex binding affinities of selected Gmf1 mutants, using the fluorescence anisotropy of Gmf1-GFP in the presence of yeast Arp2/3 complex. Gmf1-GFP bound to Arp2/3 complex with a K_D of 13 ± 2 nM (Fig 5C). This is consistent with the high affinity association revealed by analytical ultracentrifugation.

We then compared the abilities of untagged wild-type and mutant Gmf1 proteins to compete with Gmf1-GFP for binding Arp2/3 complex by monitoring the decrease in anisotropy of Gmf1-GFP. Competition with wild-type unlabeled Gmf1 demonstrated that it bound about as strongly as Gmf1-GFP, with a K_D of 10 ± 3 nM (Fig 5D and Supplemental Table S2). Gmf1-16 (11 ± 3 nM) and Gmf1-101 (10 ± 3 nM) were unaffected in their ability to bind Arp2/3 complex (Fig 5D and Supplemental Table S2), suggesting that site 2 does not play a role in directly binding Arp2/3 complex. Conversely, Gmf1-20 (210 ± 50 nM) was strongly defective in binding (Fig 5D and Supplemental Table S2). However, Gmf1-17, also in site 1 and defective in Arp2/3 inhibition, bound about as strongly as wild-type (10 ± 4 nM, Fig 5D and Supplemental Table S2) (see Discussion).

Gmf1 interacts with Arp2, Arp3 and Arc40 subunits of Arp2/3 complex

To identify Arp2/3 complex subunits directly contacting or in close proximity to GMF, we chemically crosslinked Gmf1 to Arp2/3 complex. Crosslinking between Arp2/3 complex subunits was prevented by decorating Gmf1 with sulfo-NHS before mixing with Arp2/3 complex. A number of new bands were observed that were missing from an unreacted sample of Arp2/3 complex alone, unmodified Gmf1 alone, decorated Gmf1 alone, and Arp2/3 complex mixed with unmodified Gmf1 (Fig 6A). Blotting with αGmf1 antibodies revealed several new, high molecular weight bands of discrete sizes, consistent with crosslinking to the larger subunits of Arp2/3 complex (Fig 6B). Comparison of silver stained intensity of reacted and unreacted samples of Arp2/3 complex showed that the unmodified Arp3 and ArpC1/Arc40 bands have detectable decreases in intensity. Blotting with αArp3 (Fig 6C), αArp2 (Fig 6D), and αArc40 (Fig 6E) showed that the new higher-MW bands contained each of these proteins. In contrast, very little crosslinking was apparent when blotting with αArc35 (Fig 6F). The remaining Arp2/3 complex subunits did not show detectable decreases in intensity and were not further explored. From these data we conclude that there are GMF binding sites on, or proximal to, Arp2, Arp3 and Arc40. Intriguingly, these subunits are the same ones that bind VCA [29, 31–33], and we observed that VCA can compete with GMF for binding to Arp2/3 complex in a fluorescence anisotropy based assay (Fig. S4). These results are also consistent with competitive Arp2/3 complex binding observed between *S. pombe* VCA and GMF [21].

Discussion

To address the mechanistic and structural basis for GMF's effects, we have performed a biochemical characterization, which leads to a model for its mechanism and interaction with both free Arp2/3 complex and Arp2/3 complex in the context of a filament branch junction. Although our study focused on yeast Gmf1, we extended the key findings to mammalian GMF homologues. This suggests that these Arp2/3 complex regulatory functions and mechanisms are widely conserved. Below we consider each of these conclusions.

GMF site 1 interacts with Arp2/3 complex and mediates nucleation inhibition

Our model for GMF interaction with Arp2/3 complex is highly informed by previous work on cofilin. The two actin binding sites allow each cofilin molecule to bind two adjacent subunits in an actin filament [12–14, 17, 34]. These interactions lead to severing and creation of ends that accelerate disassembly [10, 35]. Cofilin also uses site 1 to bind monomeric actin (at the barbed end of the monomer) and inhibit nucleotide exchange [26, 36, 37].

Two of our Gmf1 mutants (Gmf1-17 and Gmf1-20) were designed to mimic mutations in site 1 that disrupted cofilin binding to G actin (Figs 1 and S1) [23]. Both of these mutants disrupted the ability of Gmf1 to inhibit nucleation by Arp2/3 complex in solution (Fig 3). Since Gmf1 binds strongly to Arp2/3 complex (Fig 5; K_D = 10–13 nM) but lacks detectable affinity for monomeric actin ([19]; and S.B.P. unpublished data), these results suggest that Gmf1 inhibits nucleation by binding to the actin-related protein (Arp) subunits, Arp2 and/or Arp3, in a manner similar to how cofilin interacts with G actin. Consistent with this view, Gmf1-20 was defective in binding Arp2/3 complex when measured by fluorescence anisotropy (Fig 5). Gmf1-17 was not impaired in binding to Arp2/3 complex (Supplemental Table S2), suggesting that this less conserved part of the site 1 is not essential for the interaction (Fig 5), or does not affect the binding site reported on by the fluorescence anisotropy assay. Surprisingly, Gmf1-17 and Gmf1-20 also appear to affect nucleation inhibition in two different ways (Fig 3B), Gmf1-17 by altering the K_I of the Arp2/3 complex-Gmf1 interaction, and Gmf1-20 by changing the activity level at saturation.

However, our crosslinking data show that Gmf1 interacts with both Arp2 and Arp3 (Fig 6), and our analytical ultracentrifugation data reveals that there may be two Gmf1 binding sites on Arp2/3 complex (Fig 5). The specific defects observed for Gmf1-20 and Gmf1-17 in nucleation inhibition may therefore reflect altered interactions with two qualitatively distinct binding sites on Arp2/3 complex, which differentially contribute to nucleation inhibition. While this explanation is plausible, there are too many model parameters to allow quantitative interpretation of these surprising results at this time.

Despite these uncertainties, a qualitative structural mechanism for inhibition of nucleation by GMF can be inferred by using known structures to impose the analogy of the cofilin site 1 interaction with actin on the GMF interaction with Arp2 or Arp3. We constructed molecular models of this interaction by docking the GMFγ structure onto the structure of bovine Arp2/3 structure [27], using the structure of the twinfilin-actin complex [26] as a guide for positioning GMFγ on the barbed ends of Arp2 and/or Arp3 (Fig 7). We constructed several versions of the model, including GMF bound to Arp3 or Arp2 in the inactive conformation of the Arp2/3 complex [27, 38]. When GMF is engaged with Arp3 (Fig 7A) there are no additional contacts; when engaged with Arp2, GMF is also in contact with ArpC1/Arc40 (Fig 7B). GMF may bind to both sites at higher concentrations, explaining why both interactions were detected in our crosslinking experiments (Fig 6). There are no major clashes in either of these models, with the exception of a few residues in the Arp3 cleft, which could presumably reposition upon GMF binding. Therefore, this model is consistent with our scanning mutagenesis, crosslinking, and analytical ultracentrifugation data.

How does GMF binding inhibit nucleation? Gmf1 appears to bind to the same subunits in Arp2/3 complex as VCA, and it can be competed off of Arp2/3 complex by the addition of VCA (Supplemental Fig S4). Thus, GMF may inhibit nucleation by interfering with NPF effects on Arp2/3 complex. Furthermore, our EM data suggest that GMF alters the Arp2/3 complex conformation, shifting the distribution of particles from the closed to the open conformation (Fig 3). This is similar to the proposed mechanism of Arp2/3 complex inhibition by coronin [25].

GMF site 2 is required specifically for debranching

If Gmf1 uses site 1 to interact with the barbed end of Arp2 or Arp3, as we have modeled (Fig 7), then its site 2 would interact with the first actin subunit of the daughter filament, which forms a long pitch dimer with one of the Arps. We modeled the interaction of GMF site 2 with the first actin subunits of the daughter filament using the EM structure of cofilin-decorated actin filaments as a guide [13] (Fig 7D–E).

This model is supported by our scanning mutagenesis results. Gmf1-101 lies in a surface that overlaps with the cofilin mutant Cof1-6, which impairs F actin but not G actin binding [39]. This contact was also highlighted as being critical to cofilin-F-actin interactions in a molecular dynamics simulation [34]. Gmf1-101 was severely defective in debranching but had a near wild-type ability to inhibit nucleation by Arp2/3 complex (Fig 3), and showed normal binding to Arp2/3 complex in solution (Fig 5). These observations support our structural model, which predicts that the surface perturbed by Gmf1-101 is positioned away from Arp2/3 complex (Fig 7), and in contact with the first daughter actin (Fig 7D–E).

In sum, our model proposes that GMF debranches filaments through separate interactions with Arp3 and/or Arp2, mediated by site 1, and through interactions with actin mediated by site 2 (Fig 7F). The mechanism of debranching therefore appears to be related to actin severing by cofilin. Cofilin binding to filaments stabilizes a conformation in which actin subdomain 2 is partially displaced from the adjacent subunit, which may lead to severing

[13]. Similarly in our model, GMF binding to Arp2/3 complex at a branch junction requires partial displacement of subdomain 2 of the daughter filament actins from Arp2 and Arp3. Thus, GMF may stabilize a structure with weakened daughter filament-Arp2/3 complex interactions, leading to dissociation of the daughter filament.

A final point to consider is that while GMF is a dedicated debranching factor that does not sever filaments at other locations, ultimately its functions must be considered alongside those of cofilin. Cofilin binds cooperatively to filament sides and induces severing events at the boundaries of cofilin-decorated and bare regions, leading to filament fragmentation [10, 15, 35]. At higher saturation, this decoration also appears to disrupt Arp2/3 complex binding, inducing debranching. In the cellular context, it seems likely that both factors contribute to debranching [16, 17]. *A*n important future goal will be to determine how GMF and cofilin influence each other, and function together to regulate actin filament debranching and severing.

Materials and Methods

Detailed strain construction, protein purification, and analysis methods can be found in the Supplemental material.

Growth curves

pRS416-based plasmids carrying *GMF1* alleles were transformed into *cof1-22 gmf1Δ*. Strains were inoculated at low density in 200 μl of synthetic media lacking uracil [40] in 96-well plates and grown with agitation in a multi-well plate reader (Tecan Group Ltd., Mannedorf, Switzerland) at 34°C. Calculation of growth rates is described in the Supplemental Methods.

Total internal reflection fluorescence (TIRF) microscopy debranching assays

1 μM rabbit skeletal muscle actin (10% Oregon-green labeled), 10 nM yeast or bovine Arp2/3 complex, 100 nM dimeric VCA, and 20 nM wild type or mutant Gmf1 as indicated, were mixed in a TIRF reaction as described [41]. Detailed methods can be found in the Supplemental material.

Actin assembly assays

Actin assembly assays using pyrene fluorescence were performed essentially as previously described [41] using freshly gel-filtered rabbit skeletal muscle actin and other proteins as indicated. In Fig 3, pyrene signal was monitored in a multi-well plate reader (Tecan Group Ltd., Mannedorf, Switzerland) set to excitation wavelength 365 nm and emission wavelength 407 nm. Experiments in Fig 4 were monitored in a fluorescent spectrophotometer (Photon Technologies International, Lawrenceville, NJ). Time to achieve one half of the change in pyrene signal was determined by simple interpolation.

Fluorescence anisotropy measurements

4 nM of Gmf1-GFP was mixed with various concentrations of yeast Arp2/3 complex in 50 mM KCl, 10 mM imidazole pH 7.0, 1 mM $MgCl_2$, 1 mM EGTA, 0.5 mM DTT and 0.1 mM ATP, incubated at room temperature for fifteen minutes prior to measuring the fluorescence anisotropy of GMF by measuring polarized emission intensities at 510 nm when excited at 492 nm.

Analytical ultracentrifugation

Analytical ultracentrifugation experiments were performed in an Optima XL-I centrifuge equipped with an An50-Ti rotor (Beckman-Coulter, Indianapolis, IN). Individual sample components were gel filtered into 5 mM HEPES pH 7.0, 50 mM KCl, 1 mM $MgCl_2$, 1 mM EGTA and appropriate volumes were combined without concentration, diluting with additional buffer, and one tenth volume of the same buffer supplemented with 1 mM ATP (final ATP concentration is 100 μM). Roughly 400 μl of each sample was placed in charcoal-filled, dual-sector Epon centerpieces and allowed to equilibrate at the experimental temperature (20° C) for several hours. Absorbance at 492 nm and Rayleigh interference was monitored as the proteins sedimented at a rotor speed of 42,000 rpm. $c_k(s)$ distributions were fit to the data using SEDPHAT [28, 42, 43].

Electron microscopy

Single-particle electron microscopy was performed essentially as described [44] with some modifications. Full details can be found in the Supplemental Methods.

Chemical crosslinking analysis

Gmf1 was purified to the SOURCE15Q ion exchange step, and then 1 mL of 20 μM Gmf1 was sulfo-NHS labeled on carboxylic acids using a two-step protocol [45], and gel filtered into XLB (10 mM HEPES pH 7, 1 mM $MgCl_2$ and 50 mM KCl). 200 nM Arp2/3 complex was crosslinked to 2 μM for four hours, the crosslinking reactions were quenched with 50 mM glycine pH 9.0. Samples were resolved on SDS-PAGE gels, and imaged by silver staining or transferred to PVDF and imaged by western blot. Western blotting was performed using anti-Arp3 (y-152, Santa Cruz), anti-Arp2 (yN-16, Santa Cruz), αArc40 [46], αArc35 [47], or αGmf1 [19] primary antibodies.\

Supplementary Material

Refer to Web version on PubMed Central for supplementary material.

Acknowledgments

We are grateful to B. Nolen for providing bovine Arp2/3 complex, B. Smith for help with statistical analysis, P. Schuck and C. Brautigam for helpful discussions on the analysis of centrifugation data, L. Doolittle and J. Weinstein for technical assistance, G. Davidovich for use of the JEOL 2100 electron microscopy, and A. Bogdanov and S. Polevova for help with EM data collection. C.A.Y. was supported by a postdoctoral fellowship from the American Heart Association (Founder's Affiliate, 11POST5830010); S.B.P was supported by grants to Michael K. Rosen from the Howard Hughes Medical Institute, the NIH (R01-GM56322) and the Welch Foundation (I–1544). O.S. was supported by a Knowledge Avant-garde Award from AstraZeneka, the Ministry of Education and Science of the Russian Federation (07.514.11.4125) and RFBR grant (13-04-01570). B.L.G. was supported by a grant from the NIH (GM063691).

References

1. Rotty JD, Wu C, Bear JE. New insights into the regulation and cellular functions of the ARP2/3 complex. Nature reviews. Molecular cell biology. 2013; 14:7–12. [PubMed: 23212475]
2. Mullins RD, Heuser JA, Pollard TD. The interaction of Arp2/3 complex with actin: nucleation, high affinity pointed end capping, and formation of branching networks of filaments. Proc Natl Acad Sci U S A. 1998; 95:6181–6186. [PubMed: 9600938]
3. Welch MD, Rosenblatt J, Skoble J, Portnoy DA, Mitchison TJ. Interaction of human Arp2/3 complex and the Listeria monocytogenes ActA protein in actin filament nucleation. Science. 1998; 281:105–108. [PubMed: 9651243]

4. Machesky LM, Insall RH. Scar1 and the related Wiskott-Aldrich syndrome protein, WASP, regulate the actin cytoskeleton through the Arp2/3 complex. Curr Biol. 1998; 8:1347–1356. [PubMed: 9889097]
5. Machesky LM, Mullins RD, Higgs HN, Kaiser DA, Blanchoin L, May RC, Hall ME, Pollard TD. Scar, a WASp-related protein, activates nucleation of actin filaments by the Arp2/3 complex. Proc Natl Acad Sci U S A. 1999; 96:3739–3744. [PubMed: 10097107]
6. Rogers SL, Wiedemann U, Stuurman N, Vale RD. Molecular requirements for actin-based lamella formation in Drosophila S2 cells. J Cell Biol. 2003; 162:1079–1088. [PubMed: 12975351]
7. Rouiller I, Xu XP, Amann KJ, Egile C, Nickell S, Nicastro D, Li R, Pollard TD, Volkmann N, Hanein D. The structural basis of actin filament branching by the Arp2/3 complex. J Cell Biol. 2008; 180:887–895. [PubMed: 18316411]
8. Lappalainen P, Drubin DG. Cofilin promotes rapid actin filament turnover in vivo. Nature. 1997; 388:78–82. [PubMed: 9214506]
9. Wiesner S, Helfer E, Didry D, Ducouret G, Lafuma F, Carlier MF, Pantaloni D. A biomimetic motility assay provides insight into the mechanism of actin-based motility. J Cell Biol. 2003; 160:387–398. [PubMed: 12551957]
10. Reymann AC, Suarez C, Guerin C, Martiel JL, Staiger CJ, Blanchoin L, Boujemaa-Paterski R. Turnover of branched actin filament networks by stochastic fragmentation with ADF/cofilin. Mol Biol Cell. 2011; 22:2541–2550. [PubMed: 21613547]
11. McGough A, Pope B, Chiu W, Weeds A. Cofilin changes the twist of F-actin: implications for actin filament dynamics and cellular function. The Journal of cell biology. 1997; 138:771–781. [PubMed: 9265645]
12. Blanchoin L, Pollard TD, Mullins RD. Interactions of ADF/cofilin, Arp2/3 complex, capping protein and profilin in remodeling of branched actin filament networks. Curr Biol. 2000; 10:1273–1282. [PubMed: 11069108]
13. Galkin VE, Orlova A, Kudryashov DS, Solodukhin A, Reisler E, Schroder GF, Egelman EH. Remodeling of actin filaments by ADF/cofilin proteins. Proc Natl Acad Sci U S A. 2011; 108:20568–20572. [PubMed: 22158895]
14. Galkin VE, Orlova A, VanLoock MS, Shvetsov A, Reisler E, Egelman EH. ADF/cofilin use an intrinsic mode of F-actin instability to disrupt actin filaments. The Journal of cell biology. 2003; 163:1057–1066. [PubMed: 14657234]
15. Suarez C, Roland J, Boujemaa-Paterski R, Kang H, McCullough BR, Reymann AC, Guerin C, Martiel JL, De la Cruz EM, Blanchoin L. Cofilin tunes the nucleotide state of actin filaments and severs at bare and decorated segment boundaries. Current biology : CB. 2011; 21:862–868. [PubMed: 21530260]
16. Blanchoin L, Amann KJ, Higgs HN, Marchand JB, Kaiser DA, Pollard TD. Direct observation of dendritic actin filament networks nucleated by Arp2/3 complex and WASP/Scar proteins. Nature. 2000; 404:1007–1011. [PubMed: 10801131]
17. Chan C, Beltzner CC, Pollard TD. Cofilin dissociates Arp2/3 complex and branches from actin filaments. Curr Biol. 2009; 19:537–545. [PubMed: 19362000]
18. Poukkula M, Kremneva E, Serlachius M, Lappalainen P. Actin-depolymerizing factor homology domain: a conserved fold performing diverse roles in cytoskeletal dynamics. Cytoskeleton. 2011; 68:471–490. [PubMed: 21850706]
19. Gandhi M, Smith BA, Bovellan M, Paavilainen V, Daugherty-Clarke K, Gelles J, Lappalainen P, Goode BL. GMF is a cofilin homolog that binds Arp2/3 complex to stimulate filament debranching and inhibit actin nucleation. Curr Biol. 2010; 20:861–867. [PubMed: 20362448]
20. Ikeda K, Kundu RK, Ikeda S, Kobara M, Matsubara H, Quertermous T. Glia maturation factor-gamma is preferentially expressed in microvascular endothelial and inflammatory cells and modulates actin cytoskeleton reorganization. Circ Res. 2006; 99:424–433. [PubMed: 16873721]
21. Nakano K, Kuwayama H, Kawasaki M, Numata O, Takaine M. GMF is an evolutionarily developed Adf/cofilin-superfamily protein involved in the Arp2/3 complex-mediated organization of the actin cytoskeleton. Cytoskeleton (Hoboken). 2010; 67:373–382. [PubMed: 20517925]

22. Hess DC, Myers CL, Huttenhower C, Hibbs MA, Hayes AP, Paw J, Clore JJ, Mendoza RM, Luis BS, Nislow C, et al. Computationally driven, quantitative experiments discover genes required for mitochondrial biogenesis. PLoS Genet. 2009; 5:e1000407. [PubMed: 19300474]
23. Lappalainen P, Fedorov EV, Fedorov AA, Almo SC, Drubin DG. Essential functions and actin-binding surfaces of yeast cofilin revealed by systematic mutagenesis. The EMBO journal. 1997; 16:5520–5530. [PubMed: 9312011]
24. Ojala PJ, Paavilainen V, Lappalainen P. Identification of yeast cofilin residues specific for actin monomer and PIP2 binding. Biochemistry. 2001; 40:15562–15569. [PubMed: 11747431]
25. Rodal AA, Kozubowski L, Goode BL, Drubin DG, Hartwig JH. Actin and septin ultrastructures at the budding yeast cell cortex. Mol Biol Cell. 2005; 16:372–384. [PubMed: 15525671]
26. Paavilainen VO, Oksanen E, Goldman A, Lappalainen P. Structure of the actin-depolymerizing factor homology domain in complex with actin. The Journal of cell biology. 2008; 182:51–59. [PubMed: 18625842]
27. Robinson RC, Turbedsky K, Kaiser DA, Marchand JB, Higgs HN, Choe S, Pollard TD. Crystal structure of Arp2/3 complex. Science. 2001; 294:1679–1684. [PubMed: 11721045]
28. Balbo A, Minor KH, Velikovsky CA, Mariuzza RA, Peterson CB, Schuck P. Studying multiprotein complexes by multisignal sedimentation velocity analytical ultracentrifugation. Proceedings of the National Academy of Sciences of the United States of America. 2005; 102:81–86. [PubMed: 15613487]
29. Padrick SB, Doolittle LK, Brautigam CA, King DS, Rosen MK. Arp2/3 complex is bound and activated by two WASP proteins. Proceedings of the National Academy of Sciences of the United States of America. 2011; 108:E472–479. [PubMed: 21676863]
30. Schuck P. Diffusion of the reaction boundary of rapidly interacting macromolecules in sedimentation velocity. Biophysical journal. 2010; 98:2741–2751. [PubMed: 20513419]
31. Irobi E, Aguda AH, Larsson M, Guerin C, Yin HL, Burtnick LD, Blanchoin L, Robinson RC. Structural basis of actin sequestration by thymosin-beta4: implications for WH2 proteins. The EMBO journal. 2004; 23:3599–3608. [PubMed: 15329672]
32. Boczkowska M, Rebowski G, Petoukhov MV, Hayes DB, Svergun DI, Dominguez R. X-ray scattering study of activated Arp2/3 complex with bound actin-WCA. Structure. 2008; 16:695–704. [PubMed: 18462674]
33. Ti SC, Jurgenson CT, Nolen BJ, Pollard TD. Structural and biochemical characterization of two binding sites for nucleation-promoting factor WASp-VCA on Arp2/3 complex. Proceedings of the National Academy of Sciences of the United States of America. 2011; 108:E463–471. [PubMed: 21676862]
34. Wong DY, Sept D. The interaction of cofilin with the actin filament. J Mol Biol. 2011; 413:97–105. [PubMed: 21875597]
35. Andrianantoandro E, Pollard TD. Mechanism of actin filament turnover by severing and nucleation at different concentrations of ADF/cofilin. Mol Cell. 2006; 24:13–23. [PubMed: 17018289]
36. Blanchoin L, Pollard TD. Interaction of actin monomers with Acanthamoeba actophorin (ADF/cofilin) and profilin. The Journal of biological chemistry. 1998; 273:25106–25111. [PubMed: 9737968]
37. Carlier MF, Laurent V, Santolini J, Melki R, Didry D, Xia GX, Hong Y, Chua NH, Pantaloni D. Actin depolymerizing factor (ADF/cofilin) enhances the rate of filament turnover: implication in actin-based motility. J Cell Biol. 1997; 136:1307–1322. [PubMed: 9087445]
38. Nolen BJ, Littlefield RS, Pollard TD. Crystal structures of actin-related protein 2/3 complex with bound ATP or ADP. Proc Natl Acad Sci U S A. 2004; 101:15627–15632. [PubMed: 15505213]
39. Rodal, AA. Actin-associated Structures and Activities at the Saccharomyces Cerevisiae Cell Cortex. University of California; Berkeley: 2002.
40. Adams, A.; Gottschling, DE.; Kaiser, CA.; Stearns, T. Methods in Yeast Genetics. Cold Spring Harbor, NY: Cold Spring Harbor Laboratory Press; 1997.
41. Gandhi M, Achard V, Blanchoin L, Goode BL. Coronin switches roles in actin disassembly depending on the nucleotide state of actin. Mol Cell. 2009; 34:364–374. [PubMed: 19450534]

42. Padrick SB, Deka RK, Chuang JL, Wynn RM, Chuang DT, Norgard MV, Rosen MK, Brautigam CA. Determination of protein complex stoichiometry through multisignal sedimentation velocity experiments. Anal Biochem. 2010; 407:89–103. [PubMed: 20667444]

43. Schuck P. Size-distribution analysis of macromolecules by sedimentation velocity ultracentrifugation and lamm equation modeling. Biophys J. 2000; 78:1606–1619. [PubMed: 10692345]

44. Rodal AA, Sokolova O, Robins DB, Daugherty KM, Hippenmeyer S, Riezman H, Grigorieff N, Goode BL. Conformational changes in the Arp2/3 complex leading to actin nucleation. Nat Struct Mol Biol. 2005; 12:26–31. [PubMed: 15592479]

45. Grabarek Z, Gergely J. Zero-length crosslinking procedure with the use of active esters. Anal Biochem. 1990; 185:131–135. [PubMed: 2344038]

46. Winter DC, Choe EY, Li R. Genetic dissection of the budding yeast Arp2/3 complex: a comparison of the in vivo and structural roles of individual subunits. Proceedings of the National Academy of Sciences of the United States of America. 1999; 96:7288–7293. [PubMed: 10377407]

47. Daugherty KM, Goode BL. Functional surfaces on the p35/ARPC2 subunit of Arp2/3 complex required for cell growth, actin nucleation, and endocytosis. J Biol Chem. 2008; 283:16950–16959. [PubMed: 18381280]

48. Fedorov AA, Lappalainen P, Fedorov EV, Drubin DG, Almo SC. Structure determination of yeast cofilin. Nat Struct Biol. 1997; 4:366–369. [PubMed: 9145106]

49. Pan F, Egile C, Lipkin T, Li R. ARPC1/Arc40 mediates the interaction of the actin-related protein 2 and 3 complex with Wiskott-Aldrich syndrome protein family activators. The Journal of biological chemistry. 2004; 279:54629–54636. [PubMed: 15485833]

Research Highlights

- Functional surfaces of Gmf1 correspond to the actin-binding sites on cofilin
- Debranching requires separate surfaces on Gmf1 that bind Arp2/3 complex and actin
- Gmf1 interacts with the actin-related proteins in Arp2/3 complex
- GMF debranching activity and mechanism are conserved from yeast to mammals

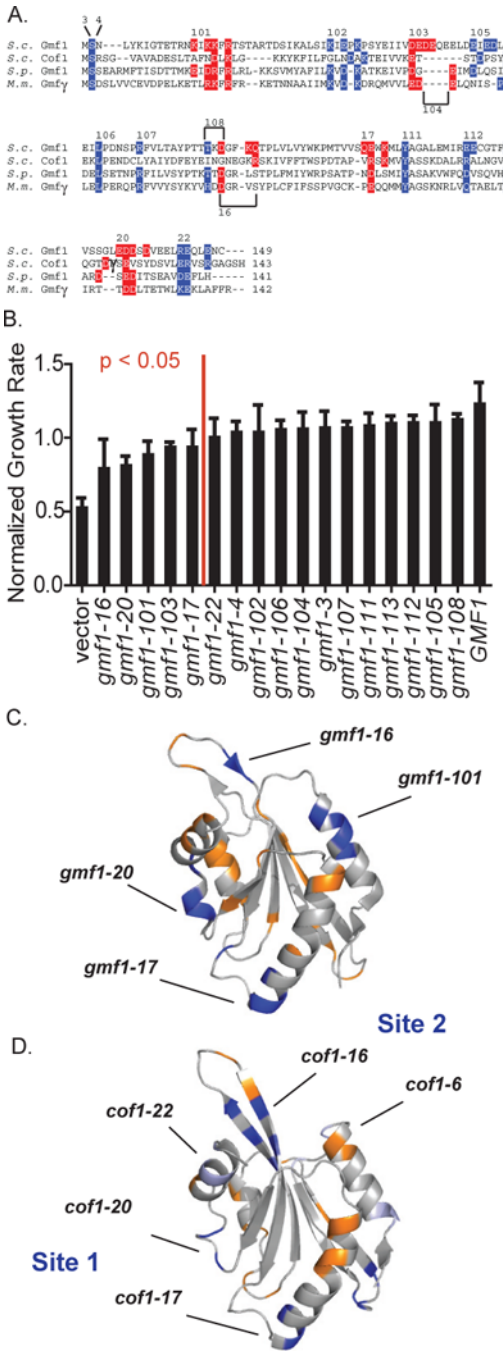

Figure 1. Site-directed mutagenesis of*GMF1*and in vivo analysis

(A) Multiple sequence alignment of *S. cerevisiae* Gmf1/Aim7, *S. cerevisiae* Cof1, *S. pombe* Gmf1, and *M musculus* Gmfγ. Allele numbers are indicated (see also Supplemental Table S1). *GMF1* alleles that have defects in vivo are colored red, *GMF1* alleles that do not have in vivo defects are colored blue. (B) Growth rates of *GMF1* alleles. OD_{600} was monitored continuously during growth in 96-well plates. Growth rates (see Supplemental Methods for calculation) were averaged from three independent experiments. Error bars represent standard deviation (C) Cartoon model of mutants mapped onto the Gmfγ structure (PDB ID: 1VKK; unpublished JCSG/PSI structure, DOI: 10.2210/pdb1vkk/pdb). Alleles that have defects in vivo are colored red and are indicated with text. Alleles that are not defective in

vivo are colored blue. (D) For comparison, cartoon model of yeast Cof1 structure (PDB ID: 1QPV [48]) with defective alleles highlighted in red.

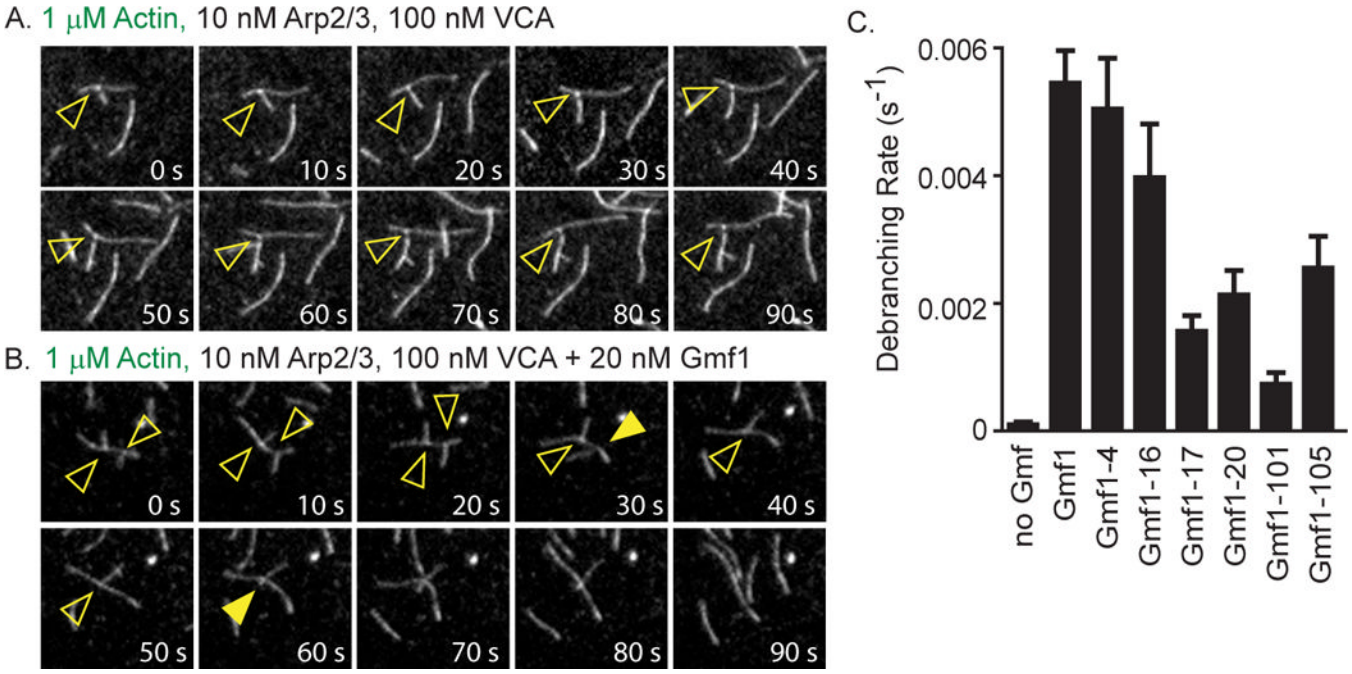

Figure 2. Debranching defects of Gmf1 mutants

A TIRF assay for actin filament debranching by Gmf1. (A–B) Samples of branch lifetime measurements in the absence (A) or presence (B) of 20 nM wild-type Gmf1. Reactions contained the indicated proteins, and frames were captured every 10 s. Branches are indicated with unfilled yellow arrowheads. Debranching events are marked by filled yellow arrowheads. (C) Data as above were used to calculate a debranching rates for each mutant Gmf1 protein (see Materials and Methods). See also Supplemental Table S2.

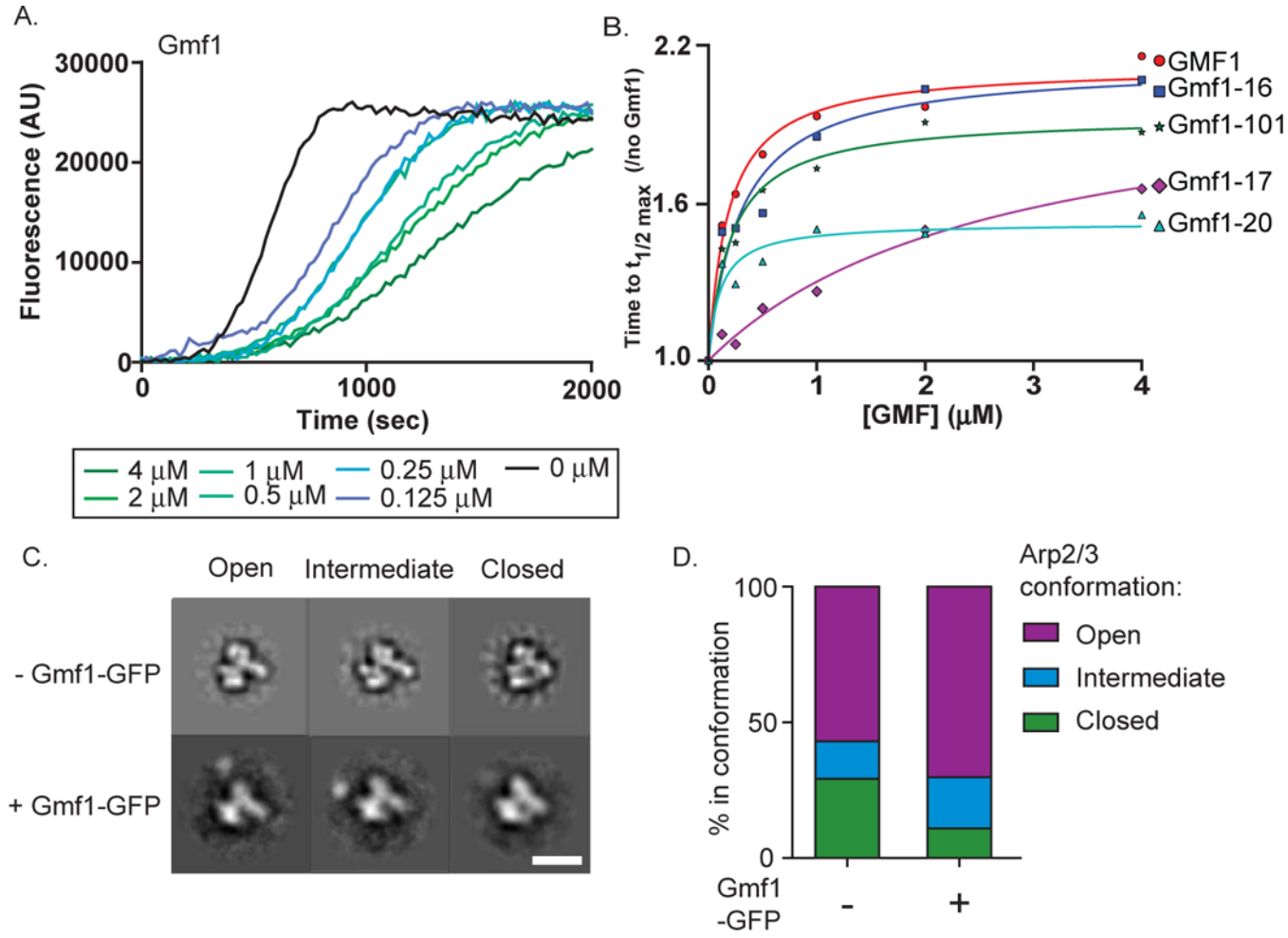

Figure 3. Inhibition of Arp2/3 complex-mediated actin nucleation by wild-type and mutant Gmf1 proteins

(A) Assembly assays containing 2 μM actin (5% pyrene labeled), 20 nM Arp2/3 complex, 200 nM GST-VCA (from yeast Las17) and variable concentrations of wild-type Gmf1. (B) Degree of inhibition by wild-type and mutant Gmf1 proteins at a range of concentrations. Time to half maximum fluorescent signal was determined for each reaction and divided by the $t_{1/2\ max}$ for a reaction without Gmf1 performed at the same time. (C–D) Gmf1 shifts the distribution of Arp2/3 complexes toward the open conformation. (C) Single-particle EM class-sum images of Arp2/3 complex alone *(top)* and Arp2/3 complex with Gmf1-GFP (*bottom*) in the open, closed and intermediate conformation. Class averages for Arp2/3 complex with Gmf1-GFP visibly bound are shown for the open and intermediate conformations, closed was not observed with Gmf1-GFP bound. Scale bar, 10 nm. (D) Analysis of relative frequencies of Arp2/3 complex conformations with and without Gmf1-GFP. Particles were counted regardless of whether Gmf1-GFP could be seen bound to Arp2/3 complex. Excluding those particles that could not be scored, n = 3758 for Arp2/3 alone and n = 5584 for Gmf1-GFP mixed with Arp2/3.

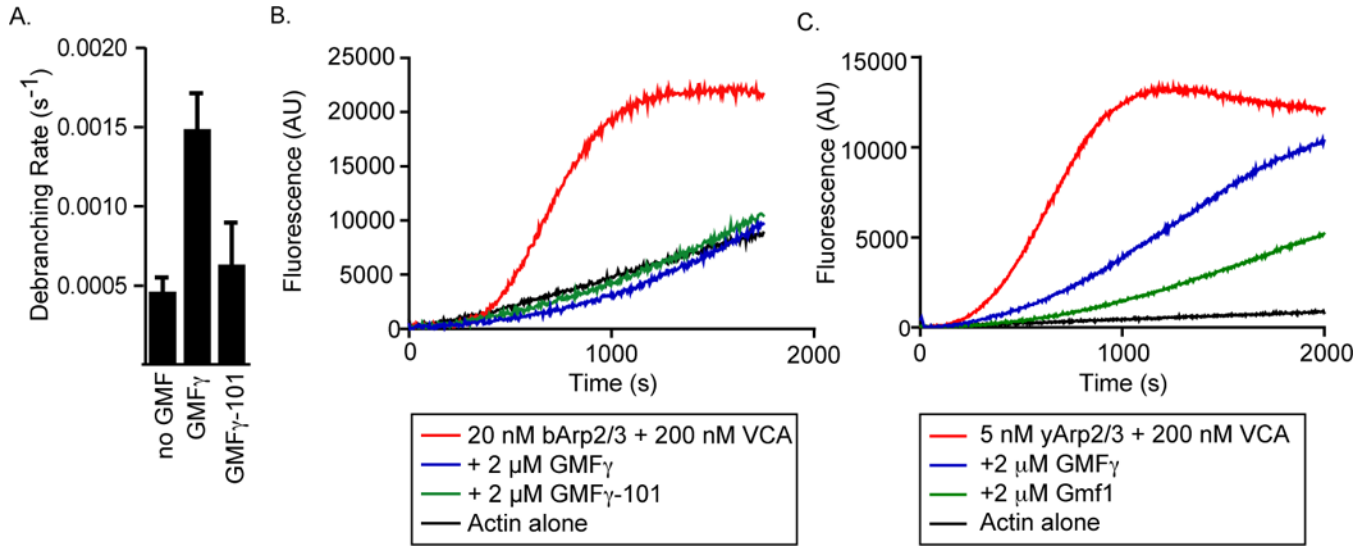

Figure 4. Mammalian GMFγ has similar debranching and nucleation inhibition activities to yeast Gmf1

(A) Debranching activities of mouse GMFγ and GMFγ-101. Debranching analysis was performed as in Fig 2 except that frames were captured every 5 s, and reactions contained bovine Arp2/3 complex. (B) GMFγ and GMFγ-101 both inhibit nucleation by bovine Arp2/3 complex and VCA. Reactions contain 2 μM actin (5% pyrene labeled), 20 nM bovine Arp2/3, 200 nM GST-VCA from human WAVE1, and 2 μM mouse GMFγ variants as indicated. (C) Mouse GMFγ also inhibits nucleation stimulated by yeast Arp2/3 complex with yeast GST-VCA.

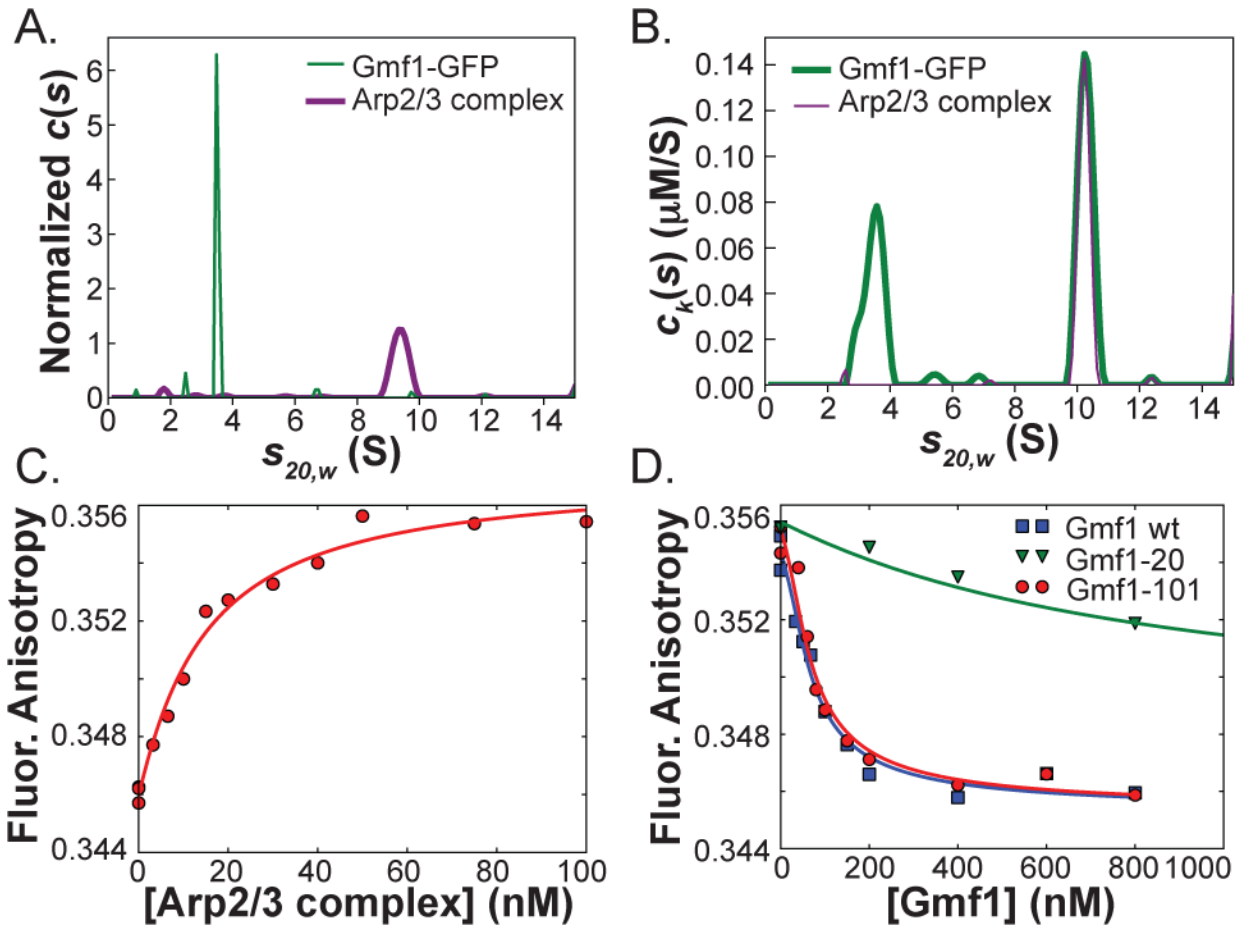

Figure 5. Binding of wild-type and mutant Gmf1 proteins to Arp2/3 complex

(A–B) Binding interactions assessed by analytical ultracentrifugation. (A) Sedimentation velocity analytical ultracentrifugation derived $c(s)$ distributions for purified yeast Arp2/3 complex and Gmf1-GFP (data in Fig. S3A–C). (B) Multi-signal sedimentation velocity data were globally analyzed (data in Fig. S3D and E) to extract $c_k(s)$ distributions for Arp2/3 complex (thin purple line) and Gmf1-GFP (thick green line). Observed sedimentation information and binding stoichiometries are reported in Supplemental Table S3, as are related analyses at different concentrations (data not shown). (C–D) Gmf1 binds to Arp2/3 complex with low nanomolar affinity. (C) Fluorescence anisotropy of 4 nM Gmf1-GFP in the presence of varying concentrations of yeast Arp2/3 complex. The fit reveals a K_D of 13 ± 2 nM. (D) Fluorescence anisotropy of 4 nM Gmf1-GFP in the presence of 40 nM Arp2/3 complex and various concentrations of unlabeled (non-fluorescent) Gmf1. The determined K_Ds are shown in Supplemental Table S2.

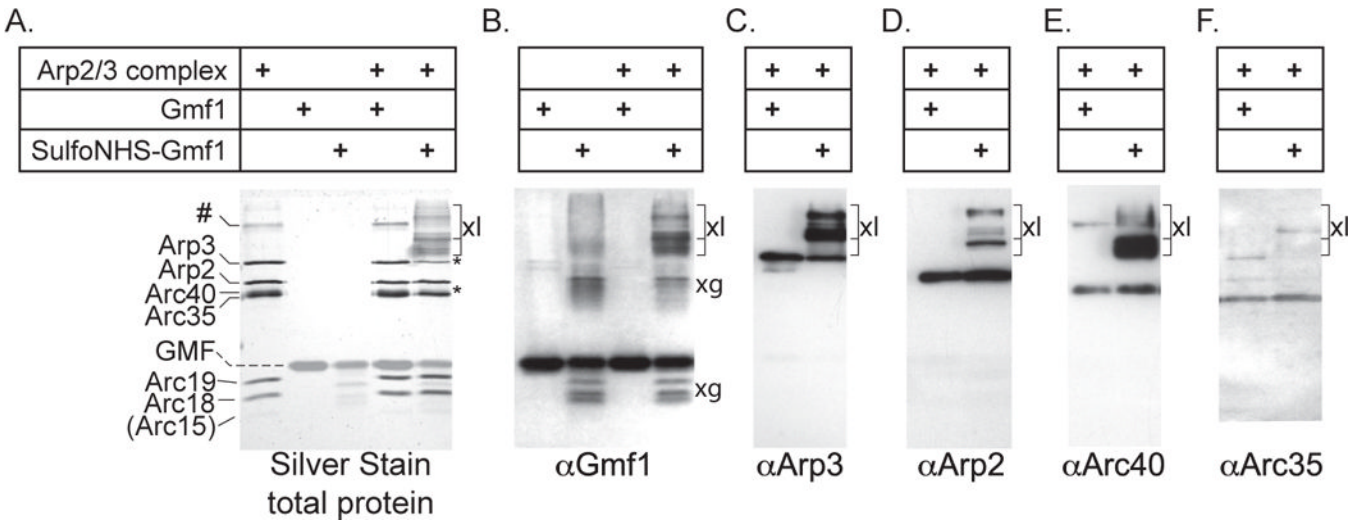

Figure 6. Gmf1 interacts with Arp2, Arc40, and Arp3

Crosslinking analysis of sulfo-NHS-decorated Gmf1 and yeast Arp2/3 complex. Components were mixed as indicated at the top of each lane. Lanes with the same components added are from the same crosslinking sample, but separate gels. Samples were separated by SDS-PAGE and either silver stained (A) or analyzed by western blotting with αGmf1 (B), αArp3 (C), αArp2 (D), αArpC1/Arc40 (E) or α ArpC2/Arc35 (F) antibodies. Gmf1 self-crosslinking products are indicated in the anti-Gmf1 blot with 'xg'. Gmf1-Arp2/3 crosslinking products are indicated with 'xl' and a bracket. A portion of Arc40 runs anomalously [49]; one of these bands is indicated by '#'. Silver stain band intensity that decreased in the crosslinked sample is indicated by '*'.

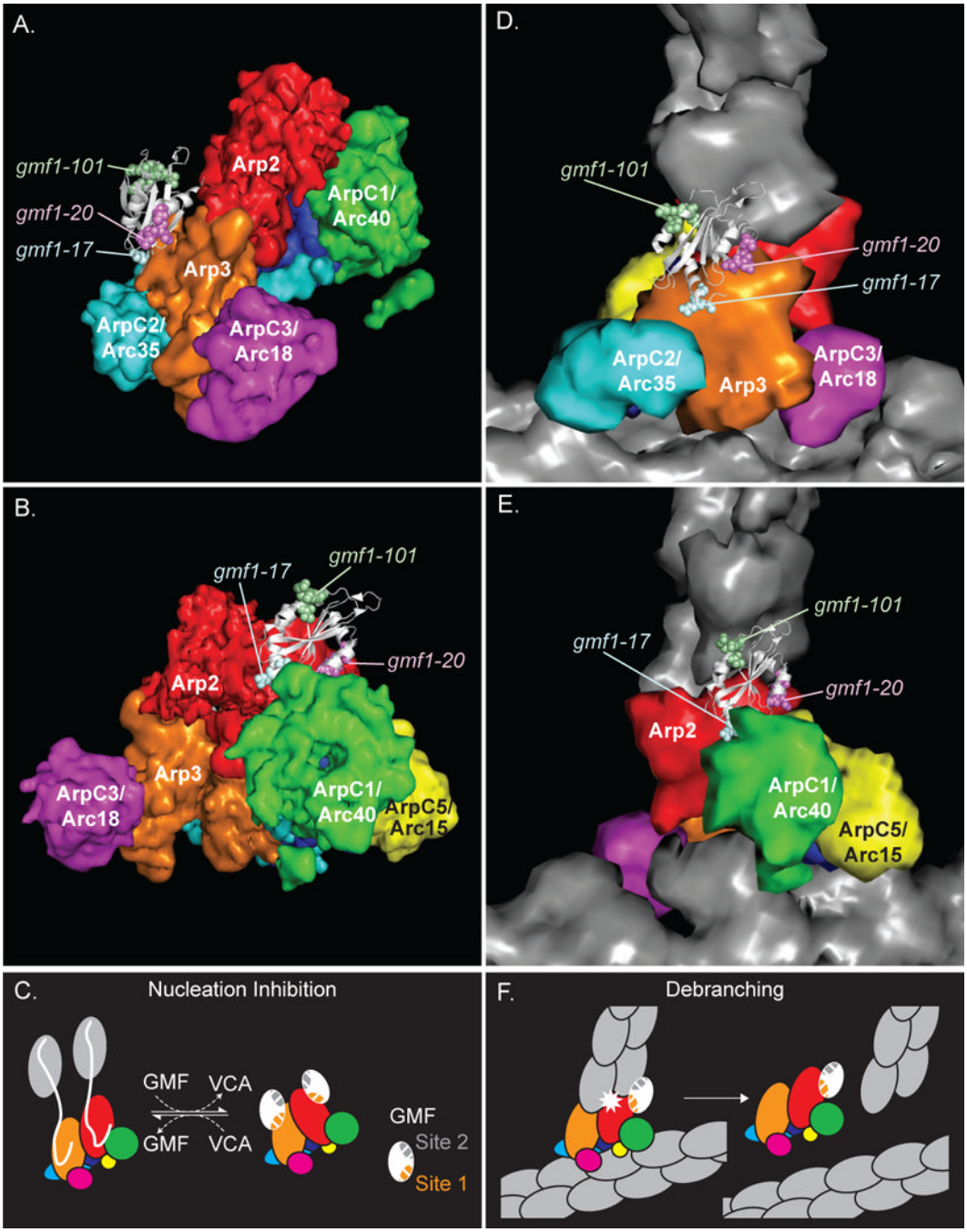

Figure 7. Model for Gmf1 interactions with Arp2/3 complex in solution and at actin filament branch junctions

(A–B) Proposed binding sites for GMF (white ribbon) on free, inhibited Arp2/3 complex (Arp2: red, Arp3: orange, ArpC1: green, ArpC2: aqua, ArpC3: purple, ArpC4: blue, ArpC5: yellow, GMF: white, shown in ribbon). There are two proposed sites, one interacting with Arp3 (A) and one interacting with Arp2 and ARPC1/Arc40 (B). Details of the modeling are in Supplemental Materials and Methods. In both models, residues from the site 1 mutations Gmf1-17 (light cyan spheres) and Gmf1-20 (light pink spheres) contact Arp2/3 complex, but residues from the site 2 mutation Gmf1-101 project away from the complex (light green spheres). Arp2/3 complex subunit surfaces are rendered using a 4 Å Gaussian blur. (C) A

model for GMF inhibition of actin nucleation mediated by WASp VCA domain and Arp2/3 complex. Inhibition is hypothesized to occur through competition between site 1 of GMF and the C-helix of VCA (represented by curvy white line) for the same binding surface, and through alteration of Arp2/3 complex conformation. (D–E) Modeling of the proposed Gmf1 binding sites in the context of the tomographic reconstruction of Arp2/3 complex-actin filament branch. Arp2/3 complex subunit surfaces are rendered using an 8 Å Gaussian blur. Actin is shown in gray surface. (F) A model of GMF-induced debranching of actin filaments, in which contacts made by both site 1 and site 2 are required. Arp2/ArpC1 binding site is shown as the contact site for simplicity.